

# Distance-of-flight spectra of charge density of ions generated with a low laser intensity

J Krása<sup>1</sup>, L Velardi<sup>2,3</sup>, A Lorusso<sup>2</sup>, D Delle Side<sup>2,3</sup>, V Nassisi<sup>2,3</sup>

<sup>1</sup>Institute of Physics, ASCR, v.v.i., Na Slovance 2, 182 21 Praha 8, Czech Republic

<sup>2</sup>LEAS, Dipartimento di Matematica e Fisica, Università del Salento

<sup>3</sup>INFN Sezione di Lecce, Via Arnesano, sn – 73100 Lecce, Italy

E-mail: krasa@fzu.cz

**Abstract.** A charge density profile of ions emitted from a laser ion source is derived from a time-resolved current of ions collected with a time-of-flight detector. This relationship between the density profile over path of ions and an ion current observed far from the ion source is based on a similarity relationship for ion currents with “frozen” charges observed at different distances from the target. In this contribution, we present distance-of-flight spectra of the charge density of ions emitted from various plasmas driven by a Compex 205 KrF excimer laser ( $\lambda=248$  nm,  $\tau_{FWHM}=23$ ns) which works at laser irradiances between  $10^8$  and  $10^{10}$  W/cm<sup>2</sup>.

## 1. Introduction

In the time-of-flight spectroscopy, the ions emitted from a laser-produced plasma are detected at the end of their flight path by means of various types of detectors. In the simplest case, the ions strike a Faraday collector, which delivers a time-resolved signal to an oscilloscope. With the purpose of obtaining information on the space properties of the expanding plasma, a number of Faraday collectors are located at various angles with respect to the target surface normal to obtain angular distributions of plasma parameters, but losing the obtained time-resolution due to e.g. time integration of ion currents.

In this paper, we present a novel method for transforming the time-resolved signal,  $S(t, L)$ , of a Faraday collector positioned at a distance,  $L$ , from the irradiated target into the ion charge density profile  $q(x, \tau)$  at a selected time,  $\tau$ , after the laser-target interaction. These distance-of-flight spectra provide a new perspective on plasma expansion.

## 2. Theory

The signal  $S_x$  of a time-of-flight detector measuring the impacted ions in  $x$ -direction depends on its response to their number, velocity or energy expressed by the term  $\alpha$ :

$$S_x(L, t, \alpha) \propto v_x^\alpha f(\vec{v}) d\vec{v}, \quad (1)$$

where  $f(\vec{v})$  is the 3-dimensional velocity distribution function and

- $\alpha = 0$  if the response is proportional to the number (density) of incident particles,
- $\alpha = 1$  if the response is proportional to the stream (current) of incident particles,
- $\alpha = 2$  if the response is proportional to the deposited energy by particles.



Substituting  $L/t$  into  $f(\vec{v})d\vec{v}$  we get the number of particles hitting the detector's area  $ds$  per  $dt$ , which is then proportional to  $f(L/t) L t^{-4}$  and  $S_x(L, t, \alpha) \sim L^{1+\alpha} t^{-(4+\alpha)} f(L/t) dt ds$ . Since the shifted Maxwell-Boltzmann distribution well describes the motion of ionized species, the detector signal can be expressed as:

$$S_x(L, t) = \kappa \frac{L^{\alpha+1}}{t^{\alpha+4}} \exp \left[ -\frac{m}{2kT} (L/t - u)^2 \right], \quad (2)$$

where  $m$  is the mass of species constituting the current  $j$ ,  $\kappa$  is the normalizing term,  $u$  is the velocity of their centre-of-mass motion directed to the ion collector,  $k$  is the Boltzmann constant and  $T$  is the ion temperature [1].

The relationship (2) enables us to determine a time  $t_{PEAK}$  at which the detector's signal reaches a maximum:

$$t_{PEAK} = \frac{L}{(\alpha+4)} \sqrt{\frac{m}{2kT}} \left( \sqrt{2(\alpha+4) + \frac{mu_{CM}^2}{2kT}} - \sqrt{\frac{mu_{CM}^2}{2kT}} \right). \quad (3)$$

The equation (3) reveals an  $\alpha$  dependence of  $t_{PEAK}$  given by the detector type as mentioned above. It is evident that the term  $(\alpha+4)^{-1}$  has substantial influence on the value of  $t_{PEAK}$ : the ion current reaches its peak value at time  $t_{PEAK-J} \cong 0.8 \times t_{PEAK-Q}$ , where  $t_{PEAK-Q}$  is the time at which the ion charge density reaches its maximum. The influence of the detector type on the time-of-flight spectra is shown in Fig. 1. The dashed line is the current density of ions  $j(L, t)$  emitted from an Ag plasma and the solid one is the corresponding time-resolved charge density  $q(L, t) = j(L, t)/v$ , i.e.  $\alpha = 0$ . The arrow shows the delay of the second peak of the ion charge density with respect to the second peak of the ion current. The ratio of both values is nearly  $t_{PEAK-J} / t_{PEAK-Q} \cong 0.8$ . Moreover, Fig. 1 shows an example of the effect of ion velocity on the ion current amplitude. When a detector, which is sensitive to the ion energy, i.e.  $(\alpha+4) = 6$ , is employed, then not only the detector signal is enhanced proportionally to the energy of ions but also the peak velocity  $v_{PEAK-E} = L / t_{PEAK-E}$  is enhanced by factor of  $\sim 1.5$  with respect to the  $v_{PEAK-Q} = L / t_{PEAK-Q}$ . The ion-energy sensitive semiconductor detectors having  $(\alpha+4) = 6$  have been advantageously used in measuring of multi-MeV ions emitted from a laser-produced plasma. [2].

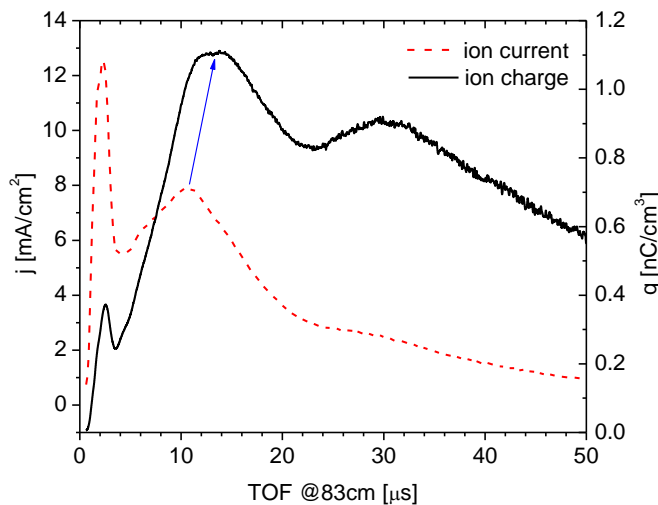


**Figure 1.** Time-resolved ion current (dashed line) and corresponding charge density (solid line) of ions emitted from Ag plasma produced with using a 350-ps iodine photo-dissociation laser PERUN operating at the second harmonic ( $\lambda=657$  nm) and delivering onto an Ag target intensity of  $5.5 \times 10^{14}$  W/cm<sup>2</sup> [3].

Taking into consideration that the time-of-flight varies with the distance as  $t = L/v$ , the relationship (1) takes a form for ion current:

$$j(L, t) L^3 = \kappa v^5 f(v). \quad (4)$$

Then the similarity relationship for currents of ions with “frozen” charges that are detected at different distances  $x$  and  $L$  is

$$j(x, \tau) x^3 = j(L, t) L^3, \quad (5)$$

where  $x/\tau = L/t$ . The similarity relationship (5) allows to determine the space-resolved ion charge density  $q_{IC} = j_{IC}/v$  by using the transformation of the time-of-flight spectrum  $j_{IC}(L, t)$  to the distance-of-flight spectrum (DOF)  $q_{IC}(x, \tau)$ , where the flight times  $t, \tau$  are related into the flight distances  $L, x$  as  $L/t = x/\tau$ , and  $L$  is the position of the IC on the  $x$ -axis. Thus, dividing both sides of the equation (3) by  $v = x/\tau$ , the DOF spectrum takes a form:

$$q(x, \tau) = j(L, \tau L/x) \tau L^3/x^4, \quad (6)$$

where time  $\tau$  is a parameter. The equation (6) transforms  $j(L, t)$  observed at a distance  $L$  from the target to  $q(x, \tau)$  at arbitrary chosen instant  $\tau$  after the laser-target interaction [4].

Supposing that ions have a Maxwell-Boltzmann velocity distribution and substituting it in (1) we obtain:

$$q(x, t) = \kappa \tau^{-4} \exp \left[ -\beta^2 \left( \frac{x}{\tau} - u_{CM} \right)^2 \right], \quad (7)$$

where  $\beta^2 = m/2kT$ .

The distance-resolved ion charge density (7) reaches a maximum at a distance:

$$x_{PEAK} = \frac{u_{CM} \tau}{2} \left( 1 + \sqrt{1 + 2/(u_{CM} \beta)^2} \right). \quad (8)$$

### 3. Experimental results and discussion

The reported measurements were performed with a Compex 205 KrF excimer laser ( $\lambda = 248$  nm,  $\tau_{FWHM} = 23$  ns) at LEAS, Lecce which works at laser irradiances from  $10^8$  to  $10^{10}$  W/cm<sup>2</sup>. The laser pulse struck the target at 70° with respect to the target surface normal. The ion current was detected with the use of Faraday cups along the target surface normal.

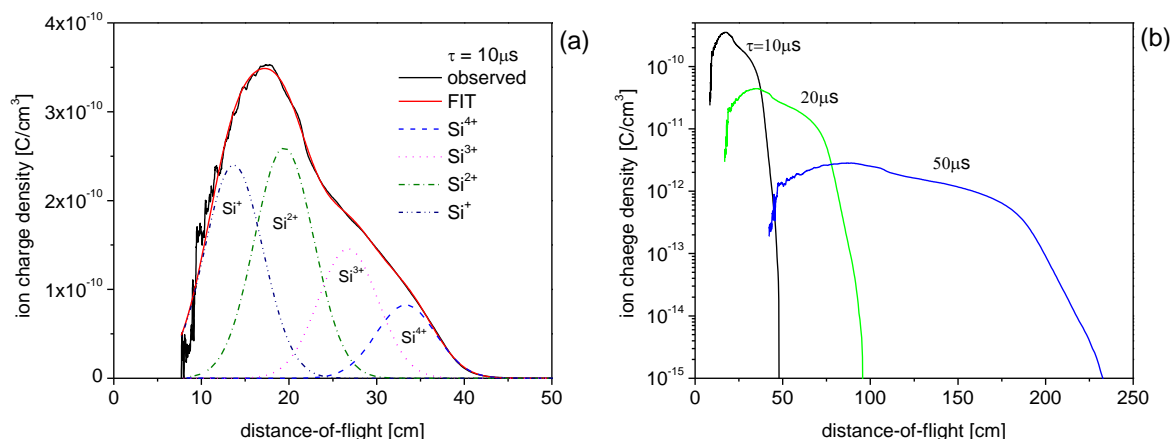


**Figure 2.** Charge density profile of  $\text{Si}^{q+}$  ( $1 \leq q \leq 4$ ) ions at 10  $\mu\text{s}$  after the laser-target interaction (a) and development of ion charge density profile in time (b). The laser fluence was 8 J/cm<sup>2</sup>.

Fig. 2 shows a DOF dependence of charge density of Si ions. Partial peaks corresponding to  $\text{Si}^{q+}$  ( $1 \leq q \leq 4$ ) ions were deconvolved from the observed signal using equation (2) [5]. Distances between the peaks are mainly given by their centre-of-mass velocity  $u_{\text{CM-}q}$  as (8) shows. The influence of the term  $u_{\text{CM-}q}\beta_q$  on  $x_{\text{PEAK-}q}$  is less than  $\sim 20\%$  to  $\sim 1\%$ , for  $q=1$  to  $q=4$ , respectively. The velocity  $u_{\text{CM-}q}$  reflects the hydrodynamic and electrostatic forces accelerating ions in the plasma [5].

Fig. 3 shows a comparison of DOF spectra of ions emitted from Al, Au, C, Cu, CuBe, Mo, Nb, Ni, Pb, Ta, and W plasmas produced with fluence of  $3 \text{ J/cm}^2$ . Fig. 3 demonstrates two well-known groups of ions: fast ionized impurities chemisorbed onto the irradiated front surface, which occupy the space in a vacuum chamber from  $\sim 40\text{-cm}$  distance-of-flight at  $10 \mu\text{s}$  after the laser-target interaction. Fig. 3 also clearly shows that for the most used target material except of C and Pb, the peak velocity of the ionized carbon is  $\sim 5\text{--}8 \times 10^6 \text{ cm/s}$  and the highest velocity of protons is  $\sim 2.1 \times 10^7 \text{ cm/s}$ , i.e. the maximum proton energy is  $220 \pm 50 \text{ eV}$ . The cut-off proton energy is lowest for the C and Pb targets.

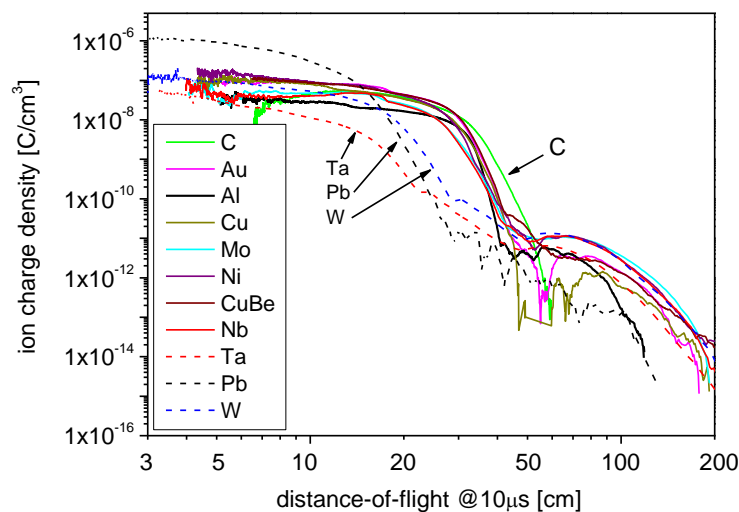


**Figure 3.** Comparison of DOF spectra of charge density of ions emitted from Al, Au, C, Cu, CuBe, Mo, Nb, Ni, Pb, Ta, and W plasmas which were produced with fluence of  $3 \text{ J/cm}^2$ .

The slower carbon ions as impurities occupy the space in a range of 40 to 80 cm from the target, as Fig. 4a shows in detail. Fig. 4b shows details of leading edges of charge density profiles of selected target materials as Nb, Mo, Cu, Au, and CuBe. There is no doubt, that except of the key parameter, which is the free electron density of the irradiated element or alloys affecting the laser pulse absorption [6,7], the melting point and other target properties affect the ion yield, as it can be emphasized by the charge density profile of the CuBe plasma. The charge density profiles of Nb and Mo are nearly identical. Similar result was obtained for Au and CuBe plasmas. The melting point of Cu, Au, and CuBe is  $1083^\circ\text{C}$ ,  $1062^\circ\text{C}$ , and  $860\text{--}1000^\circ\text{C}$ , respectively.

Another advantage of the presented novel method consists in the possibility to determine the charge density of the slowest ions having the lowest charge (in this case their  $q = 1$ ), as Fig. 3 shows. Except of lead ions, the maximum ion charge density of the other species moving with the slowest velocity varies from  $\sim 6 \times 10^{-8}$  to  $\sim 2 \times 10^{-7} \text{ C/cm}^3$ . Only slow  $\text{Pb}^+$  ions with velocity of  $5 \times 10^5 \text{ cm/s}$  reached the highest charge density of  $\sim 1.2 \times 10^{-6} \text{ C/cm}^3$  probably owing to a low value of the melting point that is  $327^\circ\text{C}$ .

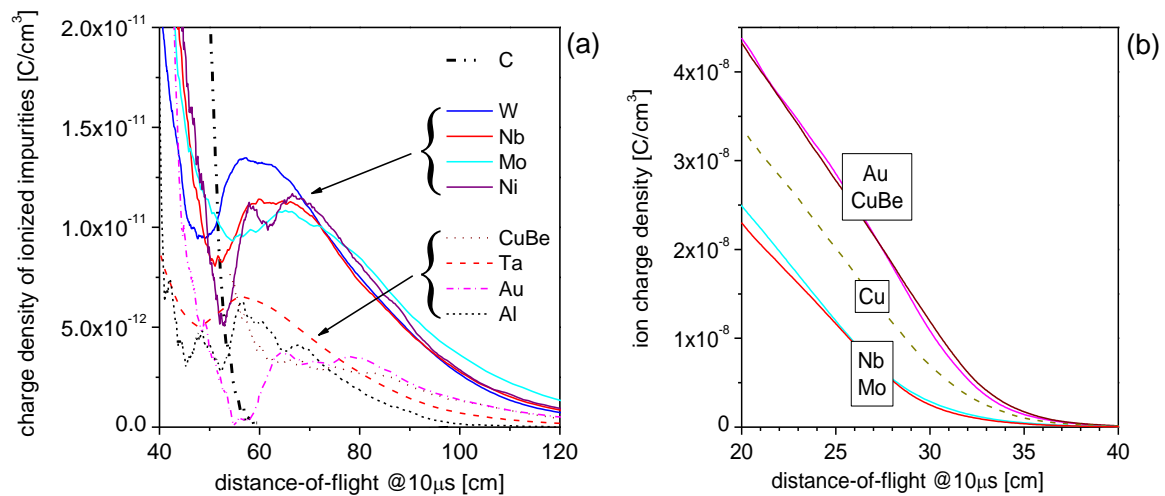


**Figure 4.** Details of Fig. 3: ionized impurities as  $\text{H}^+$  and C ions emitted from selected targets (a); leading edges of DOF spectra of the charge density of ions emitted from Au, CuBe, Cu, Mo, and Nb plasmas (b)..

#### 4. Summary

We presented a new method of the transformation of time-resolved ion currents into distance-of-flight charge density profiles. The separation of the ion charge density from the ion current and the obtained distance-of-flight spectra provide an easy way to compare the ion production efficiency in various laser-generated plasmas. Moreover, the time evolution of the distance-of-flight profiles of ion charge density was obtained.

#### Acknowledgements

The research leading to these results has received funding from the Czech Science Foundation (Grant Nos. P205/12/0454), and the Czech Republic's Ministry of Education, Youth and Sports (Project OPVK 3 - CZ.1.07/2.3.00/20.0279).

#### References

- [1] J. Krása, Appl. Surf. Sci. **272** (2013) 46 – 49.
- [2] D. Margarone, J. Krása, L. Giuffrida, A. Picciotto, L. Torrasi, T. Nowak, P. Musumeci, A. Velyhan, J. Prokúpek, L. Láská, T. Mocek, J. Ullschmied, B. Rus, J. Appl. Phys. **109** (2011) 103302.
- [3] J. Krása, L. Láská, K. Rohlena, M. Pfeifer, J. Skála, B. Králiková, P. Straka, E. Woryna, J. Wolowski, Appl. Phys. Lett. **75**, 1999, 2539-2541.
- [4] J. Krása, P. Parys, L. Velardi, A. Velyhan, L. Rýč, D. Delle Side, V. Nassisi, Laser Part. Beams (2014) **32**, 15-20.
- [5] J. Krása, A. Lorusso, V. Nassisi, L. Velardi, A. Velyhan, Laser Part. Beams **29** (2011) 113–119.
- [6] F. Caridi, L. Torrasi, D. Margarone, A. Borrielli, Laser Part. Beams **26** (2008) 265–271.
- [7] L. Torrasi, F. Caridi, L. Giuffrida, Laser Part. Beams **29** (2011) 29-37.